Numerical simulation of a new type of cross flow tidal turbine using OpenFOAM - Part II: investigation of turbine to turbine interaction

Mulualem G. Gebreslassie[☆], Gavin R. Tabor, Michael R. Belmont

College of Engineering, Mathematics and Physical Sciences
University of Exeter, North Park Road
Exeter, EX4 4QF
United kingdom

Abstract

Prediction of turbine-to-turbine interaction represents a significant challenge in determining the optimized power output from a tidal stream farm, and this is an active research area. This paper presents a detailed work which examines the influence of surrounding turbines on the performance of a base case (isolated turbine). The study was conducted using a new CFD based, *Immersed Body Force*(IBF) model, which was validated in the first paper, and an open source CFD software package OpenFOAM was used for the simulations.

The influence of the surrounding turbines was investigated using randomly chosen initial lateral and longitudinal spacing among the turbines. The initial spacing was then varied to obtain four configurations to examine the relative effect that positioning can have on the performance of the base turbine.

Keywords: IBF model, LES, Wake interaction, Spacing

1. Introduction

The study of turbine-to-turbine interaction is crucial to understand how energy shadowing of an array of devices influences energy extraction by the individual devices. Experimental studies can be carried out to investigate the wake interaction in a tidal stream farm but it is not feasible with several devices due to high investment required to cover the associated expenses. Consequently, researchers are focusing on exploring alternative methods to investigate the flow features around tidal turbines and computational fluid mechanics (CFD) modelling is currently the best option available.

Several studies have been conducted using CFD to model the flow features in and around the conventional tidal turbines. Studies by [1–5] utilized actuator disc approximation methods to investigate the flow characteristics of individual turbines and arrays. The actuator disc method is a highly simplified momentum absorption zone and has no capability of resolving the flow around each blade except reducing the momentum of the fluid as it passes through the disc [2]. A study by [1] also indicated that the vortex shedding from the edge of the disc is not similar with rotating blades and lacks swirl producing flow.

The aim of this study is therefore to demonstrate the capability of the new CFD based, *Immersed Body Force* (IBF) model, introduced in the first paper in investigating the turbine-to-turbine interactions focusing on the new type of tidal turbine, Momentum Reversal Lift (MRL) developed by Aquascientific Ltd. The investigation has been conducted in two stages. The first stage examined the performance and wake characteristics of a sin-

[☆]Corresponding author. *Telephone:* +447550747812
Email address: mgg204@ex.ac.uk (M.G. Gebreslassie)

gle turbine considered as a base case. In the second stage, a small tidal stream farm model containing a total of up to seven turbines, where one of the devices was assumed as the base case, was developed. The influence of the additional six turbines on the performance of the base case was then investigated. Different lateral and longitudinal inter-turbine spacings were used to examine the influence on the base case relative to an initially assumed spacing.

2. Computational modelling

The governing equation of the large eddy simulations (LES) and the tidal turbine modelling method, the *Immersed Body Force* (IBF), are discussed in detail in the first paper. However, a summary of the main points of the computational modelling are presented in this paper.

The LES governing equations utilized for the simulation are a combination of the filtered Navier-Stokes (NS) equations and source terms as shown in Eqn. (2). Additionally, the presence of the free surface interface between the air and water is treated through the commonly used Volume of Fluid (VOF) method, by introducing a volume fraction α and solving an additional modelled transport equation for this quantity [6]. In this study, a new source term, forcing function (F_b), was added to the existing LES model to create a momentum change in the fluid flow by the turbine blades. The complete continuity and momentum equation of the LES is defined as:
Continuity equation:

$$\frac{\partial \overline{u}_i}{\partial x_i} = 0 \qquad (1)$$

Momentum equation:

$$\frac{\partial \overline{u}_i}{\partial t} + \frac{\partial}{\partial x_j}\left(\overline{u_i u_j}\right) = -\frac{1}{\rho}\left(\frac{\partial \overline{p}}{\partial x_i} + \delta_{i1}\frac{\partial \langle P \rangle}{\partial x_1}\right)$$
$$+ \nu \frac{\partial}{\partial x_j}\left(\frac{\partial \overline{u}_i}{\partial x_j} + \frac{\partial \overline{u}_j}{\partial x_i}\right)$$
$$+ \rho g + \overline{F}_s + \overline{F}_b \qquad (2)$$

Where the bar $\overline{(.)}$ is the grid filter operator, $\overline{u}$ is the filtered velocity, $\overline{p}$ is the filtered pressure, ν is a dimensionless kinematic viscosity, δ_{i1} is the Kronecker-delta, and $\frac{\partial \langle P \rangle}{\partial x_1}$ is the driving force which vanishes if periodic inlet-outlet boundary conditions are not applied.

The MRL turbine is a development of cycloidal turbines and as such has a system of three symmetrical blades which revolve through 180° radians for every full rotation of the main shaft. This induces very complex, highly sheared internal flows plus a large scale circulation flow. Detailed modelling of such a system with complex internal motions is a good candidate for overset meshing and/or sliding mesh methods. However, the cost of these methods is high for modelling a farm scale array, hence a simplified CFD based model, IBF, was developed and validated with experimental data in the first paper. For the IBF approach, a forcing function $(\overline{F}_b)$ is used representing the force applied by the immersed body (turbine) to the fluid to create momentum change and rotational flows. The forcing function can be defined as:

$$\overline{F}_b = \overline{F}_D + \overline{F}_L \qquad (3)$$

The forcing function was added in the NS equations as shown in Eqn. (2) and a code was developed by considering drag $(\overline{F}_D)$ and lift $(\overline{F}_L)$ forces applied by the blades on the fluid flow as shown in Fig. 1. The *annular* method discussed in the first paper has been used for the investigation of surface deformation, wake states and energy shadowing between two turbines configured in series in the stream flow direction [7]. This method was also used in this study due to the advantages it has over the *blade* method in producing swirling flows and showing faster wake recovery.

3. Computational domain and boundary conditions

3.1. Computational domain set up

Figs. 2 and 3 shows a schematic representation of a horizontal plane computational domain for a single (base case) and seven turbines respectively.
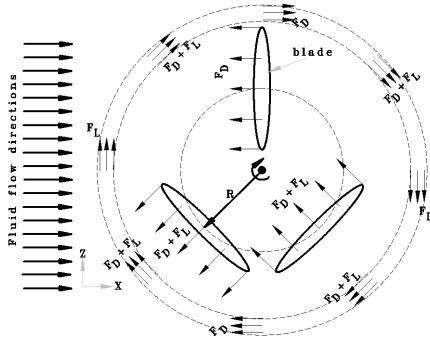
2

Figure 1: Schematic representation of the force directions of the *annular* method IBF model

The turbines were represented as a line to show their layout on the tidal farm. An investigation was carried out by considering three different sizes of computational domain, which is currently under-review for publication in another journal. The size of the domain used in this paper was therefore chosen based on that investigation. This domain is a compromise between a larger domain size which has taken longer computational time and a smaller domain which has a constraint problem that affects the wake development.
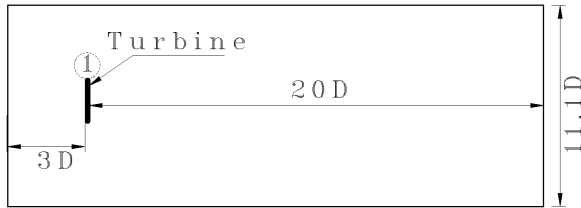

Figure 2: Single turbine schematic representation

The effects of the lateral, upstream and downstream turbines on the base turbine were analysed using four configurations by varying the lateral and longitudinal spacing. The spacing among the turbines was denoted by downstream spacing (DS), upstream spacing (US), outlet spacing (OS), Lateral spacing (LS), and width (W) as shown in Fig. 3.

Four different configurations were used according the spacing shown in table 1. The base turbine is labelled as 1 to identify from the rest of the surrounding turbines.
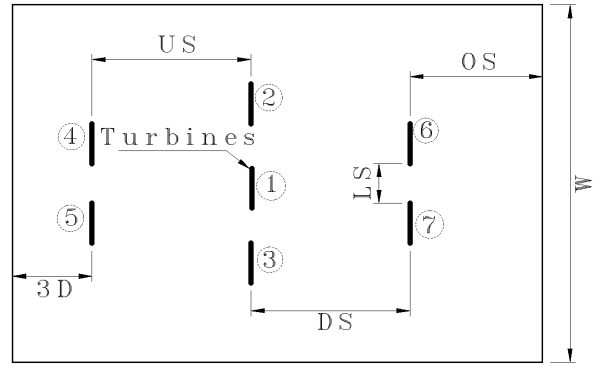

Figure 3: Seven turbine schematic representation

Config.	Spacing				
	US	DS	OS	LS	W
71	10D	10D	10D	3D	19.3D
72	10D	10D	10D	6D	25.3D
73	15D	15D	15D	3D	19.3D
74	15D	15D	15D	6D	25.3D

Table 1: Seven turbine configurations

3.2. Implementation of boundary condition

The *inlet* boundary condition used in the first paper was changed to take into consideration the change of velocity profile across the depth of the domain. This velocity field has been studied for many years and there were some arguments that say the maximum velocity occurs at the free surface as explained by [8, 9]. This argument has been challenged by many researchers [10–13] and they have proved that the maximum velocity occurs slightly below the free surface because of the resistance at the interface between the two phases, water and air. [10] had specifically described that the maximum velocity occurs in one third of the water depth from the free surface. Both the researchers described the flow as a parabolic velocity profile. Thus, at the inlet to the computational domain, a parabolic velocity field is applied to account the flow differences along the depth of the channel.

A parabolic velocity profile was implemented by [6] for a calculation of fluid flow in a tube where

the maximum velocity occurs at the centre of the tube. This code was modified in this study to match an inlet parabolic velocity profile (4a) for a channel flow based on the location of the maximum velocity given by [10] and imposed on the inlet patch of the computational domain of both the single (base case) and array of turbines. Fig. 4a shows a parabolic velocity profile extracted from the inlet boundary condition where the maximum velocity occurs slightly below the free surface (Y = 1.2625m) similar to the arguments given by the number of authors discussed before. The velocity profile above the free surface shows zero velocity as expected because this region represents the air body of the computational domain.
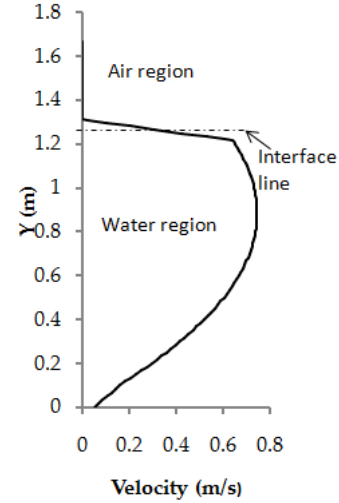
The velocity profile in the span-wise direction (horizontal plane) of the domain shows nearly constant velocity except a small fall near the wall boundaries as shown in Fig. 4b, due to the boundary interaction. The horizontal velocity profile was taken at the place where the maximum velocity occurs in the parabolic velocity profile shown in Fig. 4a. A maximum velocity of 0.746 m/s which was measured during an experimental study has been used throughout this study.
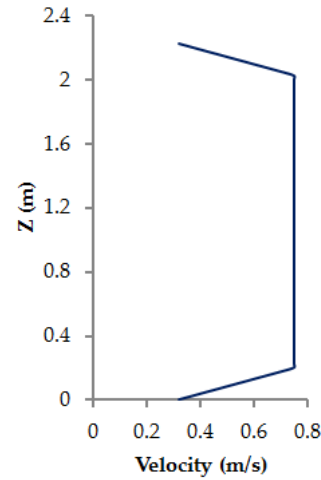
4. Data analysis methods

The analysis of the simulated data was mainly carried out by estimating the performance of the turbines and using the velocity graphs. In addition, a wavelet transform method was used to obtain more clear information on the mixing of the wake by using the velocity data extracted from the simulations as a signal. The method helps to transform the velocity signal, a one- dimensional data, into another representation which is more useful and illustrative form.

There are two types of wavelet transform, a continuous wavelet transform and a discrete wavelet transform [14]. The continuous wavelet transform has been developed by [15], where as the discrete or orthogonal transform was discovered by [16].

There are several wavelet functions developed for different applications. However, the choice of the function depends on the nature of the data and

(a) Vertical plane

(b) Horizontal plane

Figure 4: Velocity profiles at the inlet of the domain

the kind of information required to be extracted from the signal. In this paper, Daubechies orthogonal wavelets was applied to obtain the wavelet coefficients. The analysing wavelet ,ψ, used to investigate the velocity signal is defined as [17]:

$$\psi_{j,k}(x) = 2^{-j/2}\psi\left(2^{-j}x - k\right) \quad (4)$$

where: the integers j and k control the dilation and translation respectively. A discrete wavelet transform was used to compute the wavelet coef-

ficients, $T_{j,k}(x)$, of the velocity signal $u(x)$ using the analysing wavelet as [18]:

$$T_{j,k}(x) = \sum_{j} \sum_{k} u(x)\psi_{j,k}(x) \qquad (5)$$

5. Results and discussions

5.1. Base case results

The performance and wake characteristics of a single turbine were investigated and used as a base for further analysis of the influence of surrounding turbines on these parameters. Fig. 5 shows the velocity contours both in vertical and horizontal plane across the centre of the single turbine. A physically large wake (lower flow rate) can be seen immediately downstream of the turbine due to the momentum change created by the immersed body forces.

(a) Vertical plane across the centre of the turbine

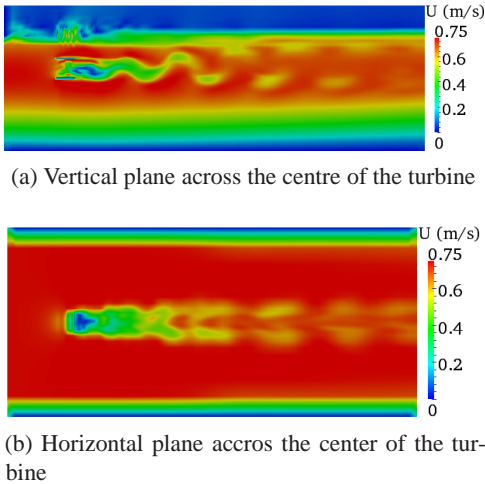(b) Horizontal plane accros the center of the turbine

Figure 5: Velocity contours of the base case

The wake characteristics were examined using both a horizontal and vertical velocity profiles. Fig. 6 shows the instantaneous velocity gradient line along the stream direction through the centreline of the turbine. It is clear from the graph that the flow rate decreases as the fluid passed through the turbine and starts to recover back further downstream. It shows particularly large flow rate deficit immediately downstream of the turbine. The wake was not

fully recovered into its initial flow rate at the end of the domain as shown in the graph.
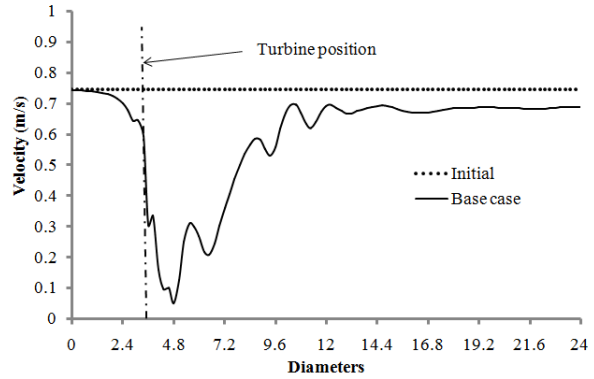

Figure 6: Centreline stream-wise velocity deficit for base turbine

The vertical velocity profile was examined at the end of the domain to obtain the length of the downstream domain required for full recovery of the wake into the initial flow rate. The flow rate was recovered to 94% of the stream flow at the end of the domain (20D), which indicates that the given domain was not enough for full wake recovery. The result shows that a 20D longitudinal spacing between turbines will create a wake interaction consequently affecting the performance of downstream turbine. Therefore, a more detailed investigation of the inevitable turbine-to-turbine interactions in a tidal stream farm is vital to obtain knowledge of all the necessary parameters as discussed in section 5.2.

To gain better understanding of the velocity fluctuations downstream of the turbine, the velocity signal shown in Fig. 7 has been analysed using the wavelet transform method. Fig. 8 shows the analysed signal and the corresponding linearly decomposed signal at 3 levels of detail coefficients and one approximation. These coefficients give a representation of the energy distribution among different scales and how it varies with the dimension of the domain.

The amplitudes of the detailed coefficients of d1, d2 and d3 are higher within and downstream of the turbine (from 2.4-16.8 diameters) and vanished afterwards. The details showed zero amplitude be-
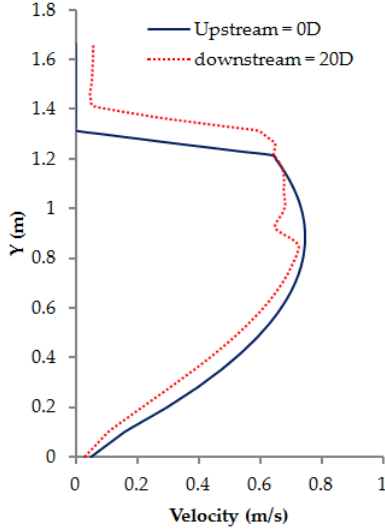
5

Figure 7: Comparison of vertical velocity profiles at the inlet and outlet of the computational domain

Figure 8: Wavelet coefficients of the centreline velocity of the base case

fore 2.4 and after 16.8 diameters especially on the fine scale d1, which indicates negligible velocity fluctuations. The wavelet decomposition analysis improved in detecting the velocity fluctuations in the stream-wise direction which is crucial to know the length of the domain where the fluctuations vanished. It gives valuable information if there is any velocity fluctuation that could reach downstream turbine, which can affect its performance and life cycle.

A comparison of the detail coefficients between the levels indicate that the amplitude was higher at d3 than d1 considering similar positions though the fluctuation was almost zero at the end of the domain in all of the levels. The high amplitude was probably due to high contribution of large length scales to the detail coefficients.

The power taken-off by the turbine was estimated at the optimum loading where a maximum power coefficient was obtained and both the averaged velocity through the turbine (u_t) and the power coefficient (C_P) are given in table 2. These two parameters were used as a base to investigate the influence of turbine-to-turbine interactions. These values represents the performance of turbine 1 when simulated in an isolated conditions and the
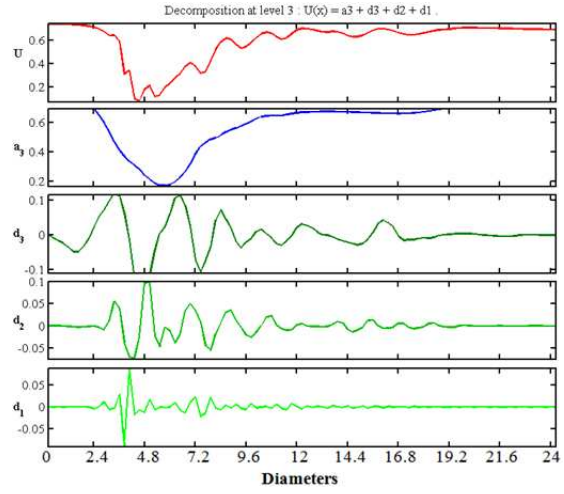
performance of the same turbine but with an additional surrounding turbines was compared in section 5.2 relative to the parameters given in the table.

No of turbines	u_t	C_P
Base case	0.47	58.9%

Table 2: Base case power coefficient

5.2. The influence of surrounding turbines

In this section, more turbines were added upstream, downstream, and on the side of the base turbine (turbine 1) to analyse the combined effect of the surrounding turbines on its performance. First, an initially assumed longitudinal and lateral spacing were used in configuration 71. These spacing were then changed to obtain three additional configurations 72, 73 and 74 in order to investigate the relative influence of these changes on the flow features.

The velocity contours from all four configurations are shown in Fig. 9. The wake of the upstream row (turbines 4 and 5) in configuration 71 interacts with the middle row (turbines 1, 2 and 3) and the mixed wake of these rows subsequently creates severe wake on the downstream row (turbines

(a) Configuration 71

(b) Configuration 73

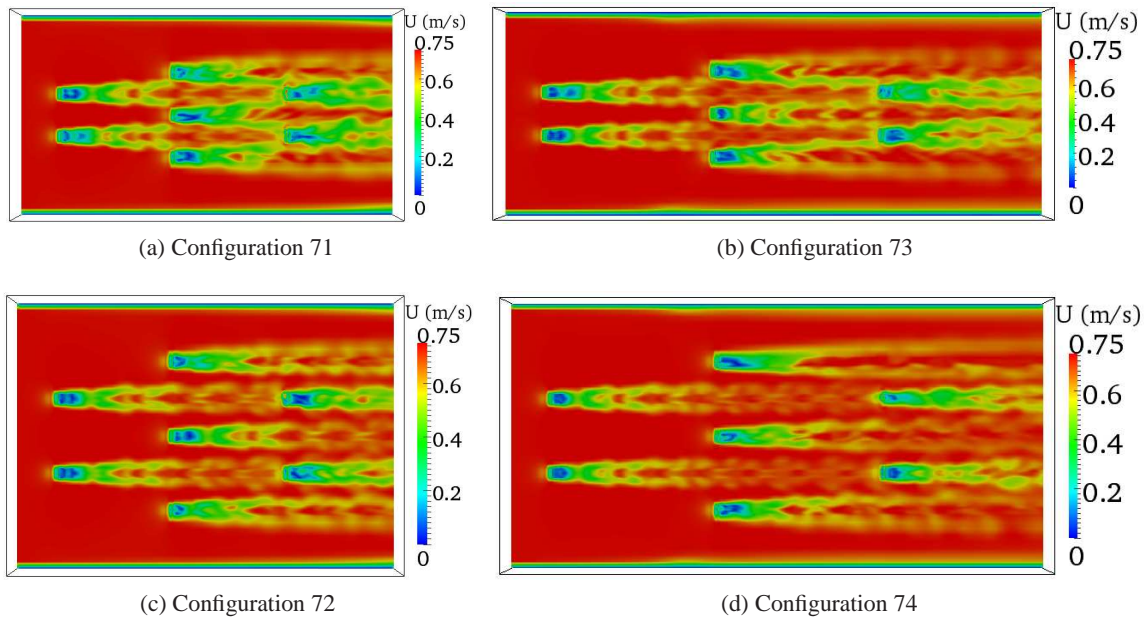(c) Configuration 72

(d) Configuration 74

Figure 9: Velocity contours in the horizontal plane across the centre of seven turbines in four configurations

6 and 7) as shown in Fig. 9a. The wake interactions of the upstream row with the middle row were minimized by increasing the lateral spacing in configuration 72 as shown in Fig. 9c. However, the wake of the upstream row still interacted with the downstream row as it flows through the bypass of the middle row due to insufficient longitudinal spacing.

The longitudinal spacing (10D) between the rows used in configurations 71 and 72 were increased to 15D in configurations 73 and 74 respectively while keeping the same lateral spacing of the former configurations. However, there was still a wake interaction among the turbines in configuration 73 (Fig. 9b) though it was improved compared with configuration 71 (Fig. 9a) which suggests that the longitudinal spacing was not enough for full recovery of the wake. The lateral spacing of configuration 73 was increased while maintaining the same longitudinal spacing and the interaction was minimised as shown in configuration 74 (Fig. 9d). The main reason of the minimal interaction in configuration 74 was that the wake of the upstream row had sufficient lateral and longitudinal spacing, which flows through the bypass without

interacting with the middle row and almost recovered back to its initial condition before it reaches the downstream row.

A one-dimensional instantaneous velocity dataset was extracted along the stream direction through the centreline of turbine 1 from the four configurations to compare with the same dataset from the base case to get a better insight to what happens to the flow through turbine 1 as shown in Fig. 10. There was an interesting observation in the four configurations immediately downstream of the upstream row (turbines 4 and 5) in which the flow accelerates especially with the small lateral spacing, configurations 71 and 73. This was due to the fact that the turbines serve as a guide creating a venturi flow between them which ultimately increases the flow rate. The other general observation was that the velocity profile at the end of the domain showed fluctuating condition while the velocity profile of the base case showed almost constant value.

The wake of the base case recovers faster than the wake of the same turbine simulated in configuration 71 as shown in Fig. 10a. This shows that turbine 1 in configuration 71 was affected by the wake

(a) Configuration 71 and base case

(b) Configuration 73 and base case

(c) Configuration 72 and base case

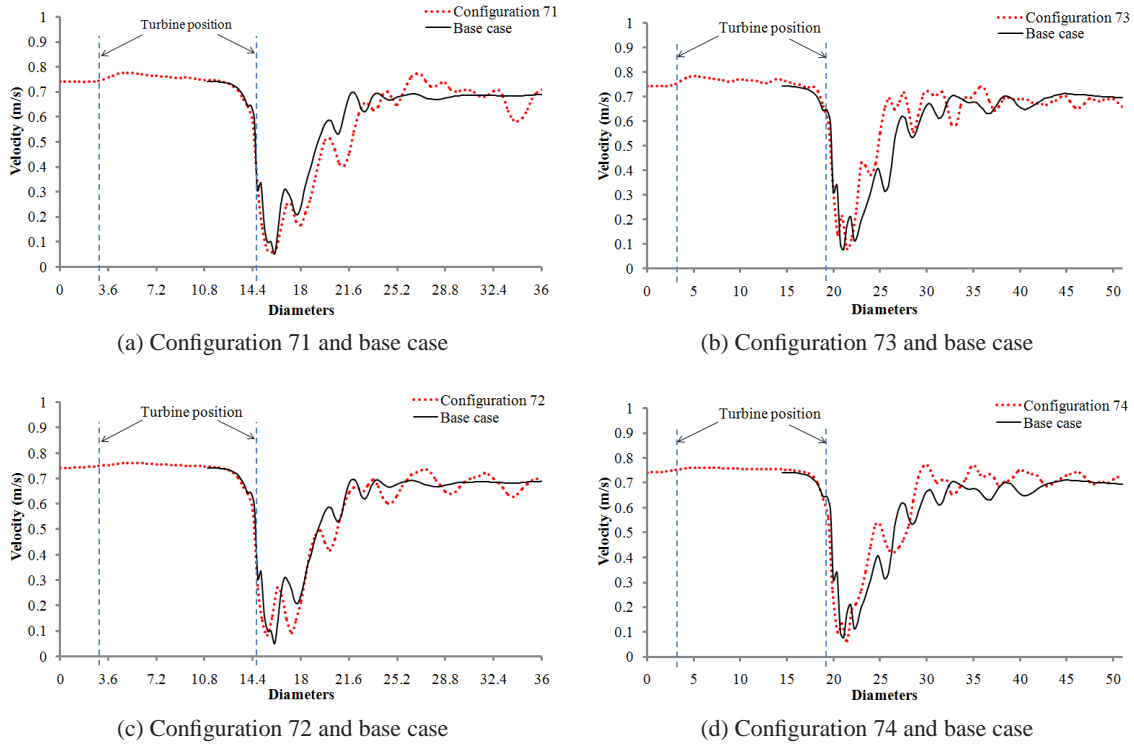(d) Configuration 74 and base case

Figure 10: Comparison of the centreline stream-wise velocity deficit through turbine 1 with the base case

of the upstream row. However, the results in configuration 72 (Fig. 10c) showed better agreement due to the increased lateral spacing, which reduced the wake interaction of the upstream row with turbine 1 but there is still a room for improvement by further increase of the lateral spacing if there is no space constraint.

In contrast, the wake of turbine 1 in configuration 73 recovers faster than the base case (Fig. 10b). A better match was obtained by increasing the lateral spacing in configuration 74 but still slightly faster than the base case as shown in Fig. 10d. The reason for this result could be a trade-off between the blockage effect and the wake interaction which increases the flow through turbine 1. This has been reflected in the power calculation discussed at the end of this section.

Fig. 11 shows the analysed signal and the corresponding linearly decomposed signals at 3 levels of detail coefficients and one approximation for the four configurations. The detail coefficients showed that the velocity fluctuations at the end of the do-

main in configuration 71 (Fig. 11a) were higher than in configuration 72 (Fig. 11c). These higher fluctuations were due to the mixing of the wake that sustains beyond the end of the computational domain, which was improved in configuration 72. Similarly, the velocity fluctuation in configuration 74 (Fig. 11d) was minimum compared with configuration 73 (Fig. 11b). Thus, the results showed some differences in the four configurations relative to each other with the change of longitudinal and lateral spacing which came due to the wake interactions.

The velocity fluctuations were higher immediately downstream of the turbine and reduced further downstream in all four of the configurations. However, high frequency fluctuations continued further downstream than in the base case (Fig. 8) which could damage the performance of any downstream turbine.

Table 3 shows the percentage changes of the flow through turbine 1 (u_t) and its power coefficient (C_p) simulated in four configuration com-

(a) Configuration 71

(b) Configuration 73

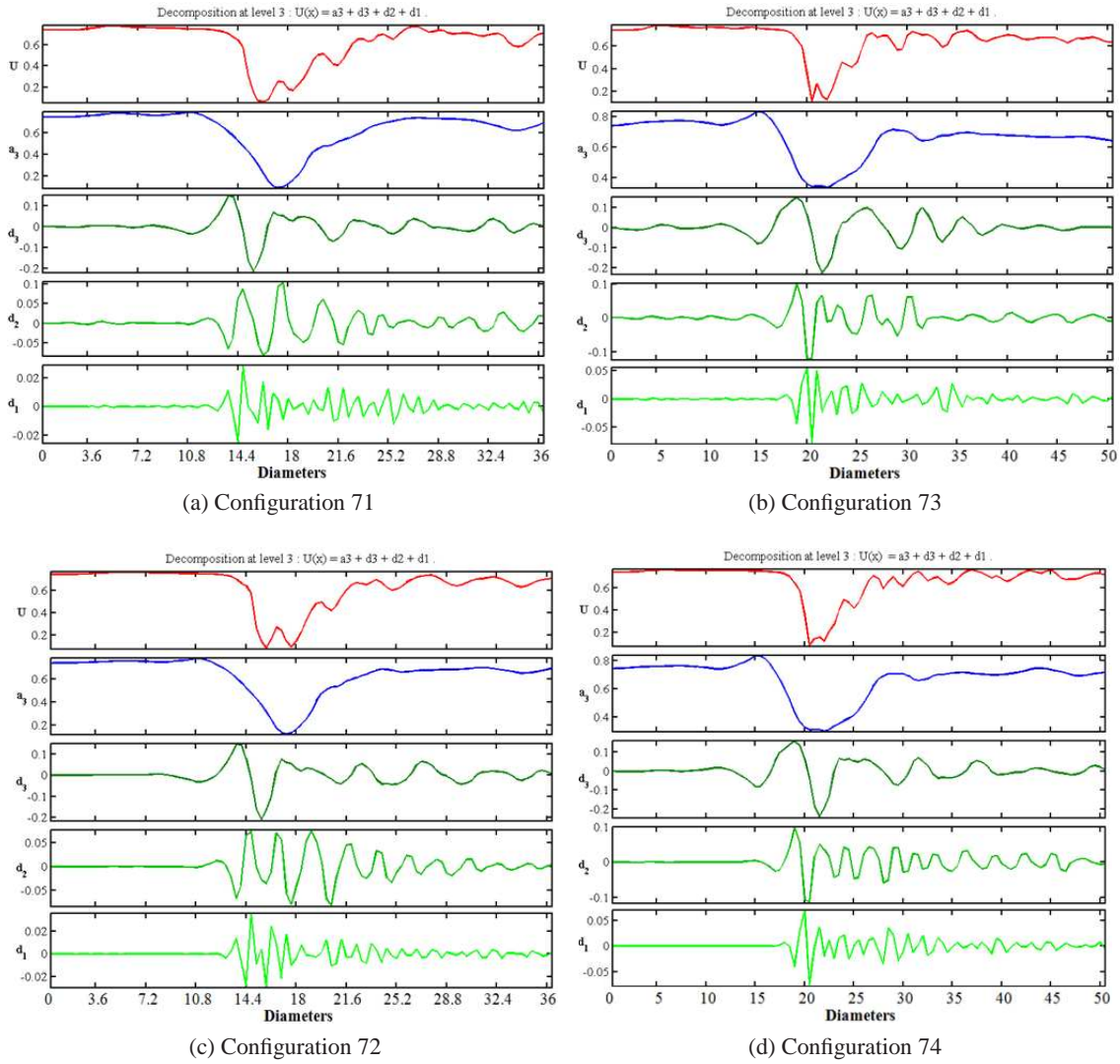(c) Configuration 72

(d) Configuration 74

Figure 11: Wavelet coefficients of the centreline velocity through turbine 1 of the four configurations

pared with the same parameters obtained from the base case. The base case conditions are given in table 2. A geometrically similar turbines have the same C_p characteristics. However, the changes of the average velocity of the downstream turbine due to the wake interaction have direct influence on the value of C_p.

The flow through the centre of turbine 1 showed different values but all negative in the four configurations. The negative values indicate a lower flow and power coefficient of turbine 1 relative to the base case, which was a prove of the effect of wake

interactions on its performance.

The power coefficient of turbine 1 in configuration 71 was 0.32% less than the base case while the same turbine in configuration 72 was less by about 0.49%. However, the performance of turbine 1 in configuration 71 was better than in configuration 72 due to a trade-off between the blockage effect and the lateral spacing.

To get a better understanding of the blockage effect, a different model was simulated using the middle row (turbines 1, 2 and 3) as shown in Fig. 12 with the lateral spacing of configuration 31 equal

to configuration 71 and configuration 32 equal to configuration 72.

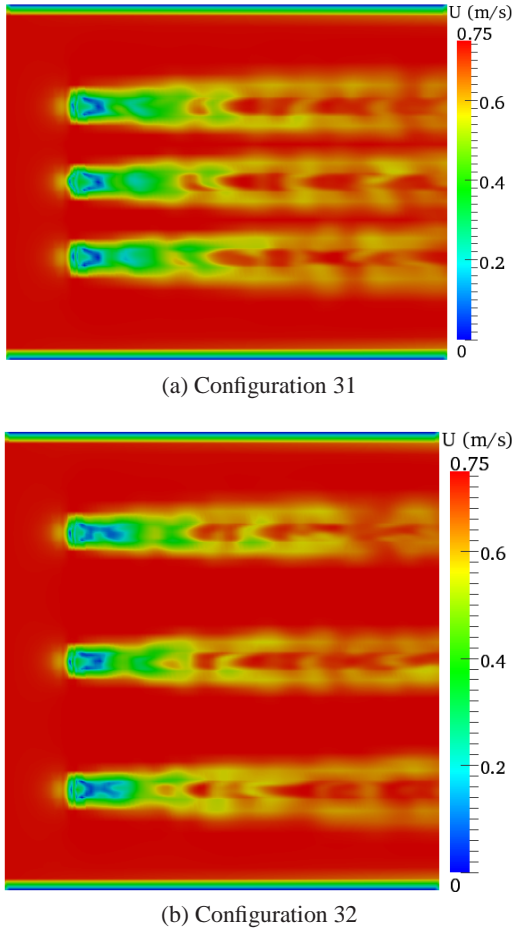(a) Configuration 31

(b) Configuration 32

Figure 12: Velocity contours in the horizontal plane across the centre of three turbines in two configurations

The power coefficient of turbine 1 in configuration 31 (Fig. 12a) was increased by 0.54%, and the same turbine in configuration 32 (Fig. 12b) increased its power coefficient by about 0.02% compared with the power coefficient obtained from the base case. This result showed that turbines configured with a small lateral spacing have positive influence on the performance of individual turbines compared with an isolated turbine due to a blockage effect. The power coefficient gets closer to the base case with the increase of lateral spacing as shown in configuration 32 with almost negligible difference of 0.02%. This proves that the perfor-

mance of turbine 1 when simulated in configuration 71 should be higher compared with the same turbine in configuration 72. However, the negative effects of the wake interaction appear to be higher than the positive influence of the blockage effect which kept the power coefficient still less than the base case in both configurations.

The power coefficient of turbine 1 in configuration 73 and 74 showed 0.23% and 0.45% less than the base case respectively. In this result, it is also proved that there is a blockage effect of the small lateral spacing as the power coefficient of turbine 1 in configuration 73 was expected to be smaller than in configuration 74. However, the power coefficient is increased in configurations 73 and 74 compared to configurations 71 and 72 due to increased longitudinal spacing, which minimised the wake interaction of the upstream row with the middle row.

No of MRL turbines		u_t (%)	C_P (%)
1		Base	case
7	configuration 71	-1.06	-0.32
	configuration 72	-1.60	-0.49
	configuration 73	-0.78	-0.23
	configuration 74	-1.46	-0.45

Table 3: Comparison of the power coefficient and the flow through the centre of the turbine

One would expect that the power coefficient of turbine 1 in configuration 74 to be close to the base case compared with the same turbine in the rest of the configurations as the wake interaction among the turbines was minimal as discussed before. However, the power coefficient of turbine 1 (-0.23%) in configuration 73 was the closest one to the base case, which was mainly due to the trade-off between the blockage effect and the wake interaction.

A change of lateral and longitudinal spacing showed some changes as expected. As the longitudinal spacing of configuration 71 changed from

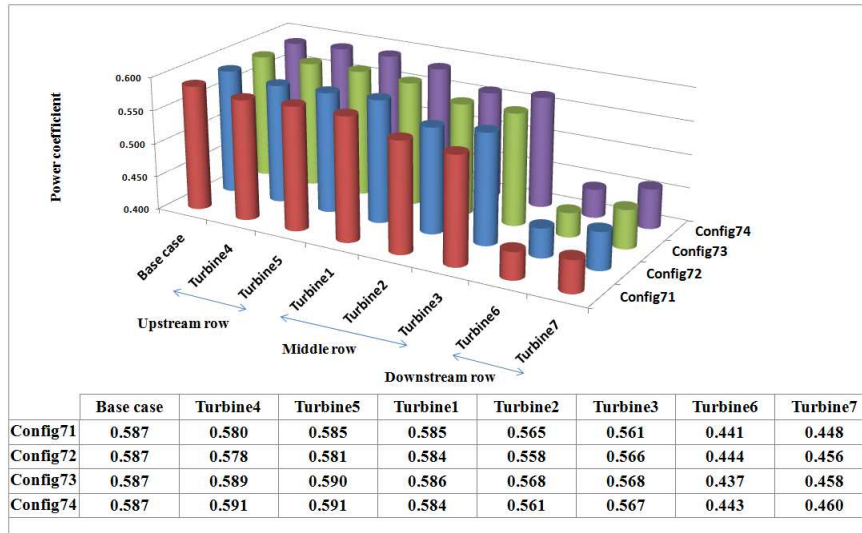|	Base case	Turbine4	Turbine5	Turbine1	Turbine2	Turbine3	Turbine6	Turbine7
Config71	0.587	0.580	0.585	0.585	0.565	0.561	0.441	0.448
Config72	0.587	0.578	0.581	0.584	0.558	0.566	0.444	0.456
Config73	0.587	0.589	0.590	0.586	0.568	0.568	0.437	0.458
Config74	0.587	0.591	0.591	0.584	0.561	0.567	0.443	0.460

Figure 13: Comparison of power output by the turbines in the base case and the four configurations

10D to 15D with the same lateral spacing, the power coefficient improved a little bit in configuration 73. Similarly, a change of longitudinal spacing from 10D (configuration 72) to 15D (configuration 74) showed an increased power coefficient. This shows a consistent result and generally it can be concluded that the larger the longitudinal spacing the better the performance of the turbines.

In contrast, laterally closer turbines showed better performance than larger lateral spacing due to the blockage effect, though this configuration will not allow the advantage of using the bypass flow in a staggered layout of devices in a tidal stream farm and can inflict a huge energy shadowing to any downstream turbines as shown in Figs. 9a and 9b. This opens the door for further detail investigation to obtain the best configuration that gives an optimized total power output from the tidal stream farm.

However, the general observations in the four of the configurations were that the power coefficient of turbine 1 showed lower value relative to the base case, which was expected due to the inevitable influence of the turbine-to-turbine interactions.

The investigation of the performance of individual turbines in the farm showed that the power coefficients decreased from the first row to the last row of the turbines as shown in Fig. 13. The power coefficients of the turbines in the last row were reduced by more than 20% in the four configurations due to the inevitable effect of the wake interaction. The power coefficients in the first row are slightly different compared with the base case, though their location is the same in the domain, due to the blockage effect of two laterally configured turbines. The downstream turbines (turbines 6 and 7) have been expected to be equally affected by the wake interaction but the result shows that the impact on the performance of turbine 6 is slightly higher. However, such kind of small discrepancy is expected due to the complexity of the simulations.

6. Conclusion

The results of the investigation of turbine-to-turbine interaction showed that a laterally close configuration could improve the performance of individual turbines due to the blockage effect, which is created by the array of turbines in the cross flow direction. However, a small longitudinal spacing between turbines can inflict a high energy shadowing between the turbines that affects the performance of downstream turbines. Therefore, a sufficient longitudinal spacing is required to minimise the wake interactions among the turbines.

11

Due to a limited availability of experimental data, the results were compared with base case simulations to understand the relative influence of additional turbines in a tidal stream farm. In addition, the study has provided necessary information on the influence of turbine-to-turbine interactions by changing the longitudinal and lateral spacing among the turbines. Thus, the work shows the capability of the IBF model in investigating the inevitable wake interactions which occurs in a tidal stream farm

Bibliography

[1] Harrison, M., Batten, W., Myers, L., Bahaj, A.. Comparison between CFD simulations and experiments for predicting the far wake of horizontal axis tidal turbines. Renewable Power Generation, IET 2010;4(6):613–627.

[2] Gant, S., Stallard, T.. Modelling a tidal turbine in unsteady flow. In: Proceedings of the Eighteenth (2008) International Offshore and Polar Engineering Conference. 2008, p. 473–479.

[3] Bahaj, A., Myers, L., Thomson, M., Jorge, N.. Characterising the wake of horizontal axis marine current turbines. In: Proceedings of the 7th European wave and tidal energy conference. 2007,.

[4] MacLeod, A., Barnes, S., Rados, K., Bryden, I.. Wake effects in tidal current turbine farms. In: International Conference on Marine Renewable Energy-Conference Proceedings. 2002, p. 49–53.

[5] Batten, W., Bahaj, A.. CFD simulation of a small farm of horizontal axis marine current turbines. In: Proceedings World Renewable Energy Congress WREC IX. Elsevier Science; 2006,.

[6] Ltd, O.. User guide. http://www.openfoam.com/docs/user/; 2011.

[7] Gebreslassie, M., Tabor, G., Belmont, M.. CFD simulations for investigating the wake states of a new class of tidal turbine. Renewable Energy and Power Quality Journal 2012;(10, Paper No. 241).

[8] Fischer, H.. Longitudinal dispersion and turbulent mixing in open-channel flow. Annual Review of Fluid Mechanics 1973;5(1):59–78.

[9] Kirkgoz, M., Ardiclioglu, M.. Velocity profiles of developing and developed open channel flow. Journal of hydraulic engineering 1997;123:1099.

[10] Gordon, L.. Mississippi river discharge. RD Instruments, San Diego, Calif 1992;.

[11] Yang, S., Tan, S., Lim, S.. Velocity distribution and dip-phenomenon in smooth uniform open channel flows. Journal of hydraulic engineering 2004;130:1179.

[12] Chaudhry, M.. Open-channel flow. Springer Verlag; 2008.

[13] Chiu, C., Tung, N.. Maximum velocity and regularities in open-channel flow. Journal of hydraulic engineering 2002;128(4):390–398.

[14] Farge, M.. Wavelet transforms and their applications to turbulence. Annual Review of Fluid Mechanics 1992;24(1):395–458.

[15] Grossmann, A., Morlet, J.. Decomposition of hardy functions into square integrable wavelets of constant shape 1984;.

[16] Lemarié-Rieusset, P., Meyer, Y.. Ondelettes et bases hilbertiennes. Revista Matematica Iberoamericana 1986;2(1):1–18.

[17] Addison, P.. Wavelet transforms and the ecg: a review. Physiological measurement 2005;26:R155.

[18] Tzanetakis, G., Essl, G., Cook, P.. Audio analysis using the discrete wavelet transform. In: Proc. Conf. in Acoustics and Music Theory Applications. 2001,.